

See discussions, stats, and author profiles for this publication at: <https://www.researchgate.net/publication/257143506>

# Anirban Biochemistry VT18

DATASET · SEPTEMBER 2013

---

READS

42

5 AUTHORS, INCLUDING:



[Harini Mohanram](#)  
Nanyang Technological University

18 PUBLICATIONS 230 CITATIONS

[SEE PROFILE](#)



[Anirban Bhunia](#)  
Bose Institute

67 PUBLICATIONS 915 CITATIONS

[SEE PROFILE](#)



[Surajit Bhattacharya](#)  
Nanyang Technological University

69 PUBLICATIONS 1,225 CITATIONS

[SEE PROFILE](#)

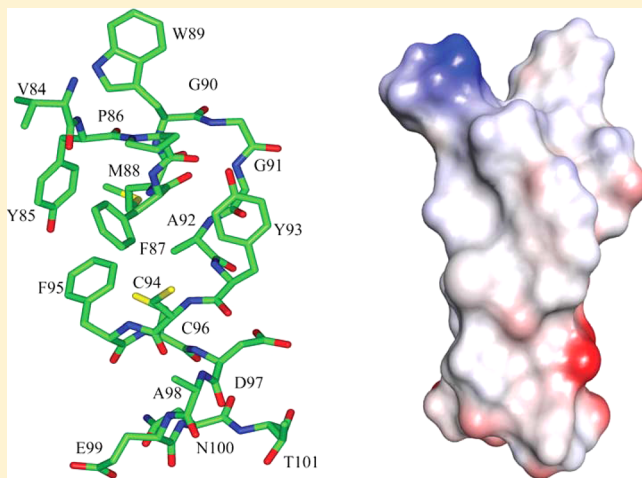
## NMR Structure, Localization, and Vesicle Fusion of Chikungunya Virus Fusion Peptide

Harini Mohanram, Alyssa Nip, Prerna N Domadia, Anirban Bhunia,<sup>#</sup> and Surajit Bhattacharjya\*

School of Biological Sciences, Division of Structural Biology and Biochemistry, Nanyang Technological University, Singapore 637551

Supporting Information

**ABSTRACT:** The virus–host cell fusion process is mediated by a membrane anchored viral fusion protein that inserts its hydrophobic fusion peptide into the plasma membrane of the host cell, initiating the fusion reaction. Therefore, fusion peptides are an important functional constituent of the fusion proteins of enveloped viruses. In this work, we characterize the fusion peptide or VT18 ( $V^{84}YPFMWGGAYCFCDENT^{101}$ ) of Chikungunya virus (CHIKV) using NMR and fluorescence spectroscopy in zwitterionic lipid environments. Our results demonstrate that the VT18 peptide is able to induce liposome fusions in a pH independent manner and interacts with the zwitterionic lipid vesicles. The NMR derived three-dimensional structure of VT18, in solution of dodecylphosphocholine (DPC) micelles, is typified by extended or  $\beta$ -type conformations for most of the residues, whereby residues M88-W89-G90-G91 adopt a type I  $\beta$ -turn conformation. Strikingly, the aromatic side chains of residues Y85, F87, Y93, and F95 in the VT18 structure are found to be well-packed forming an aromatic core. In particular, residue F87 is situated at the center of the aromatic core establishing a close proximity with other aromatic side chains. Further, the aromatic core residues are also involved in packing interactions with the side chains of residues M88, C94. Paramagnetic relaxation enhancement NMR, using spin labeled doxyl lipids, indicated that the aromatic core residues of VT18 are well inserted into the micelles, whereas the polar residues at the C-terminus may be surface localized. The atomic resolution structure and lipid interactions of CHIKV fusion peptide presented here will aid to uncover the fusion mechanism by the type II viral fusion proteins.



Enveloped viruses protect their genetic materials (DNA or RNA) from the environment by a lipid bilayer. This lipid bilayer is acquired from the host cell membrane during the process of maturation, assembly, and budding of the virus. Consequently, a new cycle of infection requires a fusion of the lipid membrane of virus with the plasma membrane of host cell.<sup>1–5</sup> The cell–cell fusion delivers the genetic materials of the virus into the cytoplasm of the infected host.<sup>1–5</sup> The lipid bilayer of virus contains transmembrane proteins those are involved in the membrane fusion and also for binding to the cellular receptors.<sup>1–5</sup> The fusion protein plays a major role in virus host cell fusion undergoing a large conformational change.<sup>1,2</sup> It is generally considered that the large and irreversible conformational change of the fusion protein occurring upon membrane insertion facilitates in overcoming the free energy barrier of fusion reaction.<sup>1,2</sup> The virus membrane fusion may occur at the plasma membrane at neutral pH which is triggered by the binding of the virus to the cell receptors.<sup>6–9</sup> By contrast, the membrane fusion reaction can also take place after cellular internalization, through the receptor mediated uptake by the endocytic pathway, of viruses, e.g., influenza viruses, alphaviruses, and flaviviruses.<sup>10–13</sup> A mildly acidic condition of endosome activates the fusion

protein causing virus membrane fusion.<sup>11–14</sup> The activation of fusion proteins, taking place either at low pH or receptor binding, exposes a hydrophobic peptide segment, termed fusion peptide or fusion domain.<sup>1,2,14–16</sup> Insertion of the fusion peptide into the plasma membrane of the host cell is vital for the initiation of the cell fusion process.<sup>14–16</sup> High resolution structures, by X-ray crystallography, of a number of fusion proteins have been determined in their prefusion and postfusion states. On the basis of these structures, the viral fusion proteins are categorized into two major classes, type I and type II.<sup>4,5,17,18</sup> The type I fusion proteins, observed in influenza virus, HIV and SARS virus, are typified by a trimeric assembly of  $\alpha$ -helical coiled coil hairpins in the postfusion state.<sup>4,5,17,18</sup> On the other hand, the type II fusion proteins, determined in flaviviruses and alphaviruses, are found to be trimers of hairpins composed of  $\beta$ -sheets in the post fusion state.<sup>4,5,17,18</sup> A third set or type III fusion protein, found in vesicular stomatitis virus and herpes simplex virus, is also

Received: July 5, 2012

Revised: September 13, 2012

Published: September 14, 2012



characterized by trimers of hairpins albeit formed both by the helical coiled-coil and  $\beta$ -sheets structures.<sup>5,19</sup> Collectively, these structural studies have provided critical information of the assembly of fusion proteins and insight toward the mechanism of cell fusion. However, the interactions of fusion proteins with the cell membrane have been inferred indirectly, since the structures of fusion proteins could not be determined in complex with the lipid membranes. In order to gain insights into the membrane fusion process, several research groups have utilized fusion peptides, predominantly from the type I fusion proteins, for structural and functional investigations in lipid environments.<sup>20–26</sup> These studies have shown that the isolated fusion peptide can display fusogenic activity. NMR spectroscopy, both in solution and solid states, has been extensively used for structural characterization of fusion peptides.<sup>27–35</sup> Toward this, three-dimensional (3-D) structures of a number of fusion peptides have been determined in lipid, DPC or SDS, micelles, by solution NMR spectroscopy.<sup>27–33</sup> Notably, NMR studies revealed helical hairpin or helical boomerang conformations of the fusion peptide of influenza virus HA2.<sup>27,30</sup> However, straight or kinked helical conformations were obtained for the fusion peptides of type I fusion proteins including HIV and SARS virus.<sup>28,29,31</sup>

It is noteworthy that similar studies of the fusion peptides from type II fusion proteins are highly limited. Recently, the NMR structure, in DPC micelles, was reported for the fusion peptide from type II fusion protein of dengue virus belonging to the class of flavivirus.<sup>36</sup> However, type II fusion peptides of the family alphaviruses are yet to be structurally characterized in complex with lipid membranes. Chikungunya virus (CHIKV), a mosquito-borne alphavirus, utilizes type II fusion protein for the virus cell fusion.<sup>37,38</sup> CHIKV has caused infection of millions of people in Africa, Asia, and Europe in recent years.<sup>38</sup> Infection by CHIKV in humans is typified by symptoms of high fever, rash, and severe arthritis, the hallmark feature of the disease.<sup>37,38</sup> CHIKV has been causing a significant health problem in humans and drug development is highly essential.<sup>39</sup> The structural glycoprotein E1 of alphaviruses is responsible for fusogenic activity, whereas glycoprotein E2, derived from furin cleavage, of a precursor protein p62 into E2 and E3, is involved in receptor binding.<sup>40–43</sup> The E1 and E2 proteins form a heterodimer, at the neutral pH, burying the fusion peptide.<sup>41–43</sup> Under the acidic endosomal environment, the E1/E2 heterodimer dissociates and the E1 protein undergoes conformational changes into  $\beta$ -sheet homotrimers following insertion of the fusion peptide into the plasma membrane.<sup>44–47</sup> Recently, crystal structures are determined for the heterodimer of E1/p62 and matured E1/E2/E3 complexes of CHIKV glycoproteins.<sup>47</sup> In order to better understand the process of membrane fusion of alphaviruses, in this work, we have determined the micelle-bound 3-D structure, liposome fusion and interactions of the fusion peptide VT18 of CHIKV.

## MATERIALS AND METHODS

**Peptide and Lipids.** VT18 peptide was purchased from GL-Biochem (Shanghai, China). Crude peptide was further purified by HPLC Waters, and the molecular weight of the peptide was verified by mass spectrometry. 1,2-Dimyristoyl-sn-glycero-3-Phosphocholine (DMPC), Rho-PE (*N*-(lissamine rhodamine B-sulfonyl) dioleoylphosphatidylethanolamine) (Rho-PE), and NBD-PE (*N*-(7-nitrobenz-2-oxa-1,3-diazol-4-yl)dioleoylphosphatidylethanolamine) were obtained from Avanti polar lipids (Alabaster, AL). Spin-labeled lipids 5-

doxyl-stearic acid (5-DSA), 16-doxyl-stearic acid (16-DSA), and Triton-X-100 were purchased from Sigma (St. Louis, MO). Perdeuterated dodecylphosphocholine (DPC-*d*<sub>38</sub>) was obtained from Cambridge Isotope Inc.

**Preparation of Large Unilamellar Vesicle (LUV).** DMPC lipid solution of 5 mM was prepared in a 2:1 chloroform/methanol mixture. A thin film of lipid was obtained by evaporation of the solvent under a stream of nitrogen gas. The lipid film was freeze-dried promptly and rehydrated in a 10 mM sodium phosphate buffer solution. The LUV was prepared following freeze-thaw and extrusion through two stacked of 100 nm polycarbonate filters (Avanti polar lipids, Alabaster, AL). The size of LUV was checked using dynamic light scattering (Malvern zeta sizer Nano ZS, Malvern, UK) measurements.

**Intrinsic Tryptophan Fluorescence Experiments.** Fluorescence measurements were carried out using a Cary Eclipse fluorescence spectrophotometer (Varian, Inc.). Peptide and LUV samples were prepared in a 10 mM sodium phosphate buffer solution, pH 5.0. The binding of the peptide to the DMPC LUV was probed using intrinsic tryptophan fluorescence emission whereby a fixed concentration, 5  $\mu$ M, of VT18 peptide was titrated with different concentrations of LUVs with lipid/peptide ratios of 4, 8, 32, 64, 128, 256, and 512. Fluorescence spectra were recorded with an excitation wavelength of 280 nm, and emission signal was collected from wavelength of 300–400 nm. A band-pass of 5 nm was used both for the excitation and emission wavelengths. In order to minimize inner filter effect and possible light scattering from LUVs, a cuvette of 0.1 cm path length was used for the fluorescence experiments. An equilibrium dissociation constant ( $K_d$ ) of the interactions between the fusion peptide with the DMPC LUVs was estimated from the change of fluorescence emission intensity from a single site binding model using Origin 6.1 (Origin laboratories, Northampton, MA).

**Lipid Mixing by the Fusion Peptide.** VT18 induced vesicle fusion or lipid mixing was investigated using standard probe dilution assay detecting fluorescence resonance energy transfer (FRET) between NBD-PE (donor) and Rho-PE (acceptor).<sup>48</sup> For these experiments, two different types of LUVs were prepared. Unlabeled LUVs were made using solely DMPC lipid and labeled LUVs were prepared by mixing DMPC (5 mM) with 1 mol % of each of NBD-PE (0.05 mM) and Rho-PE (0.05 mM) lipids. FRET experiments were carried out for VT18 peptide in 10 mM sodium phosphate buffer either at pH 5.0 or pH 7.5 in a cuvette of 0.1 cm path length. A stock solution of 1 mM of VT18 peptide was prepared in dimethyl sulfoxide. A basal fluorescence emission of NBD probe was recorded by mixing 100  $\mu$ M of unlabeled LUVs with 25  $\mu$ M of labeled LUVs. The fluorescence emission of NBD was monitored at 530 nm with an excitation wavelength of 470 nm. A band-pass of 5 nm was fixed both for the excitation and emission wavelengths. Increasing concentrations of VT18 peptide, at the molar peptide/lipid ratios of 0.2, 0.4, 0.6, and 0.8, were added to the above mixture of LUV solution and emission intensity of NBD was monitored. Control experiments were also carried out whereby only dimethyl sulfoxide was added to the mixed LUV containing solutions. The percentage of lipid mixing was calculated using the equation: % of lipid mixing =  $[(F - F_0)/(F_{max} - F_0)] * 100$ , where  $F_0$  and  $F$  represent fluorescence intensity of the NBD probe in the absence or presence of peptide respectively.  $F_{max}$  is the

maximum fluorescence intensity observed for NBD after the addition of 10% Triton-X-100.

**NMR Experiments.** NMR data were collected on a Bruker DRX 600 MHz spectrometer, equipped with cryo-probe and pulse field gradients. NMR data processing and analyses were carried out using the programs TOPSPIN (Bruker) and SPARKY, respectively. One-dimensional (1-D) proton NMR spectra of VT18 were acquired at 0.2 mM, 0.3 mM, and 0.5 mM peptide concentrations at temperatures of 298, 303, and 310 K whereby lyophilized powder of VT18 was dissolved either in 125 mM or 200 mM perdeuterated DPC solutions in water, at pH 5.0 containing 2 mM tris(2-carboxyethyl) phosphine (TCEP) as reducing agent.

Because of the favorable spectral quality, 2D NMR studies of VT18 (0.5 mM) were further carried out in aqueous solution containing 125 mM perdeuterated DPC, at pH 5.0 with 2 mM TCEP at 310 K. All NMR samples also contain 10% D<sub>2</sub>O for lock and 1 mM DSS as an internal reference of chemical shifts. The two-dimensional (2-D) <sup>1</sup>H-<sup>1</sup>H TOCSY (mixing time; 80 ms) and <sup>1</sup>H-<sup>1</sup>H NOESY (mixing time, 150 ms, 200 ms) spectra were acquired with 2K × 512 complex points using WATERGATE for water suppression and the States-TPPI for quadrature detection at the t<sub>1</sub> dimension. Spin labeled lipids, 5-DSA and 16-DSA, induced resonance perturbation studies were carried out by obtaining 2D TOCSY spectra of VT18 either in the absence or presence of 1 mM doxyl lipids. Stock solutions, 10 mM, of 5-DSA and 16-DSA were made in deuterated methanol. The intensities of the HN/C<sup>a</sup>H cross-peaks of amino acids in TOCSY spectra of VT18 were estimated before and after addition of the paramagnetic probes and the ratio of remaining amplitudes for 5-DSA and 16-DSA were calculated.

**Structure Calculation.** An ensemble of micelle-bound structures of VT18 was determined based on NOE-driven distance constraints. The intensities of NOE cross peaks, from NOESY spectra collected with a mixing time 150 ms, were categorized into strong, medium, and weak and translated into inter proton upper bound distance of 3.0, 4.0, and 5.0 Å, respectively. The lower bound of the inter proton distance was fixed to 2.0 Å. The backbone dihedral angle ( $\phi$ ) was varied from -30° to -120° for nonglycine residues to restrict the conformational space. NMR structures of VT18 were iteratively calculated from an extended polypeptide chain using Cyana 2.1<sup>49</sup> program. Twenty lowest energy structures represented the final structural ensemble. MOLMOL, PyMOL, and Insight II softwares were used to view and examine the structures. The stereochemistry of structures was determined using Procheck.<sup>50</sup>

## ■ RESULTS AND DISCUSSION

**Fusogenic Activity of the VT18 Peptide.** The fusion peptide segment of CHIKV was assigned for residues 84–101 in the full-length E1 glycoprotein.<sup>46</sup> Notably, the amino acid sequences of the fusion peptide region are highly conserved among several alphaviruses.<sup>46</sup> We have used the probe dilution assay<sup>48</sup> to examine fusogenic activity of the fusion peptide VT18 of CHIKV at pH 5.0 and 7.5. In separate experiments, fluorescence emission from NBD was monitored while mixtures of unlabeled DMPC LUV and DMPC LUV containing fluorescently labeled lipids; NBD-PE (energy donor) and rhodamine-PE (energy acceptor) were titrated with increasing concentrations of peptide. In the event of fusion between unlabeled and labeled LUVs the fluorescence emission intensity of NBD would increase as a result of reduced energy transfer between NDB and rhodamine.<sup>48</sup> Figure 1A shows

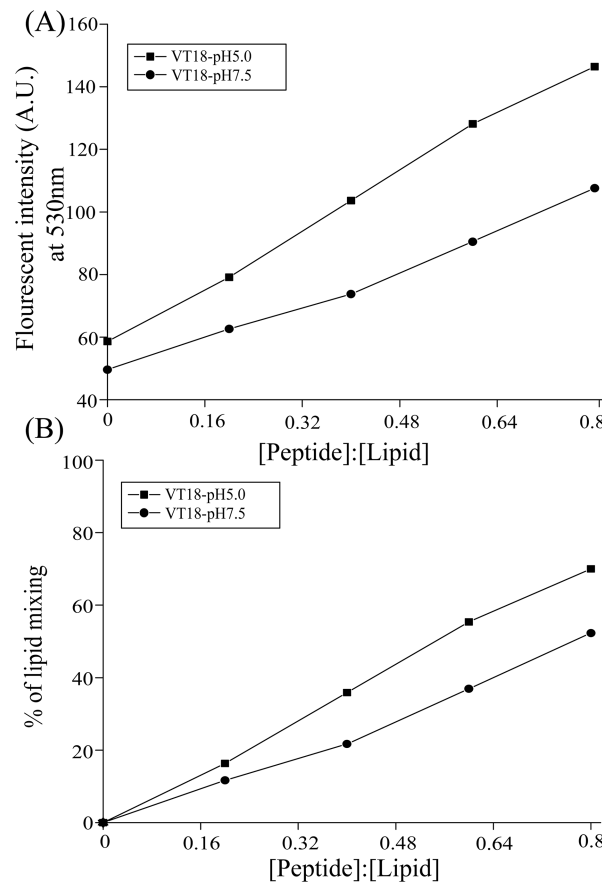


**Figure 1.** (A) Plots showing the changes of fluorescence emission intensity of NBD-PE at 530 nm at pH 5.0 and 7.5 at different molar ratio of the peptide/lipid obtained from probe dilution assays. Peptide aliquots were added to a mixture of labeled DMPC LUVs containing 1 mol % of each NBD-PE and Rho-PE and unlabeled DMPC. The dequenching of fluorescence emission of NBD in the presence of VT18 peptide indicated fusion between the labeled and unlabeled LUVs. (B) Dose dependence of lipid mixing of DMPC LUVs by VT18 peptide at pH 5.0 and 7.5. The maximal values of NBD-PE fluorescence emission intensity yielded after the inclusions of VT18 peptide were plotted as a function of the peptide/lipid molar ratio. The fluorescence intensity of NBD-PE upon addition of 10% Triton-X-100 was referred to as 100%. Fluorescence experiments were carried out in 10 mM sodium phosphate buffer, pH 5.0 or pH 7.5. The excitation wavelength was fixed at 467 nm and emission was recorded at 530 nm.

fluorescence emission intensity of the NBD-PE at 530 nm as a function of the peptide/lipid molar ratio. As evident, additions of VT18 peptide, either at pH 5.0 or pH 7.5, have yielded an enhancement in the intensity of fluorescence emission of the NBD-PE, indicating intervesicular fusion (Figure 1A). However, a somewhat higher fluorescence intensity increase of the NBD-PE can be seen at pH 5.0 in comparison to that of at pH 7.5. Further, the extent of lipid mixing caused by the fusion peptide was quantified with relative to the detergent, Triton X-100 (Figure 1B). The VT18 peptide has rendered 65% and 55% lipid mixing at the peptide/lipid ratio of 0.8, at pH 5.0 and pH 7.5, respectively (Figure 1B). Taken together, these results demonstrate that the fusion peptide, VT18, of CHIKV can independently function in membrane fusion without the rest of the E1 protein. Moreover, the fusogenic activity of the fusion peptide appears to be largely pH independent. Notably, the 3-D structure of the E1–E2 complex demarcated that the fusion

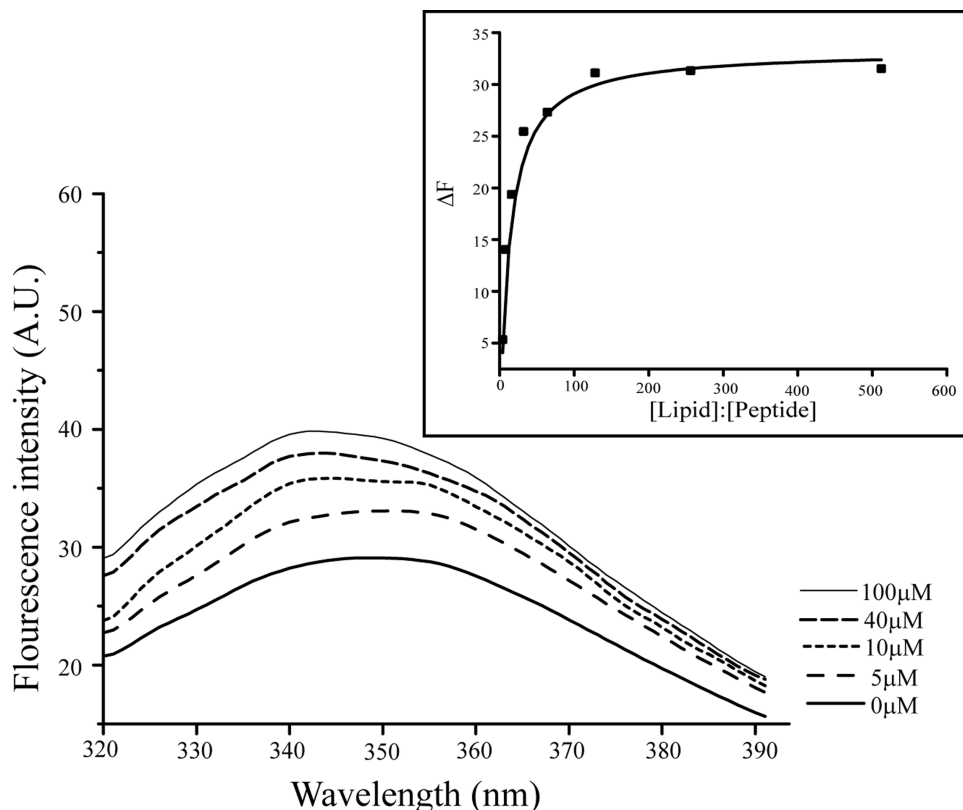


**Figure 2.** Intrinsic tryptophan fluorescence emission spectra of VT18 in the free solution and in the presence of different concentrations of DMPC LUVs. Fluorescence experiments were performed in 10 mM sodium phosphate buffer, pH 5.0 with a peptide concentration of 5  $\mu$ M. (inset) Plot shows increase in the fluorescence intensity ( $\Delta F$ ) of Trp at the different molar ratios of lipid/peptide. The data were fitted into a set of single site binding mode to determine the dissociation constant ( $K_d$ ) value of the interactions between DMPC LUVs and VT18.

peptide segment is buried at the interface of E2 protein whereby several His residues of E2 are in close proximity with the fusion peptide segment.<sup>46</sup> These His residues of E2 may be critically involved as the pH sensor for the activation of the fusion protein at lower pH.<sup>46</sup>

**Interactions of the VT18 Peptide with LUVs by Intrinsic Trp Fluorescence.** The primary structure of the VT18 fusion peptide contains a single Trp residue at the position 89. Interactions of VT18 with DMPC LUVs were examined by the intrinsic Trp fluorescence experiments (Figure 2). The emission maximum of Trp residue of VT18, in free solution, was shifted toward the longer wavelength of 350 nm, typically observed for a solvent exposed fluorophore (Figure 2). The emission maximum of Trp residue showed an enhancement of fluorescence intensity and a shift toward the shorter wavelength, 342 nm at 100  $\mu$ M LUVs, upon stepwise additions of DMPC vesicles (Figure 2). The increased quantum yield with the concomitant blue shift of emission spectra of Trp residue of VT18 demonstrates an insertion of Trp into the hydrophobic milieu of the zwitterionic DMPC lipid vesicles. The extent of solvent exposure of Trp residue of VT18 was further investigated by means of quenching with acrylamide in free solution and in complex with LUVs. There was a limited quenching of Trp fluorescence in the presence of DMPC LUVs, indicating the Trp residue of VT18 is rather buried inside lipid vesicles (Supporting Information, Figure S1). Further, an equilibrium dissociation constant ( $K_d$ )  $\sim$  9  $\mu$ M, of the interactions of VT18 with DMPC LUVs was estimated from the change of Trp fluorescence emission intensity (Figure 2 inset). It is well-known that Trp plays an important role in

anchoring membrane active peptides, including fusion peptides,<sup>27–29,36</sup> and transmembrane proteins into lipid bilayers.<sup>27–29,36,51,52</sup> Collectively, fluorescence studies indicated that the Trp residue of the fusion peptide is inserted into the zwitterionic DMPC lipid vesicles.

**NMR Studies of VT18 in DPC Micelles.** Smaller size detergent micelles, DPC or SDS, are convenient systems for structural analyses of membrane active peptides and integral membrane proteins.<sup>53–55</sup> Fast tumbling of the micellar complex in solution is often favorable for proton NMR studies of short peptides. Thereby, structures of a number of fusion peptides in solution are largely determined in lipid micelles. We have reconstituted VT18 peptide into the detergent solution of DPC micelles for NMR structural analyses. It may be noted that cell membranes of higher organisms including humans are rich in zwitterionic lipid molecules. Thus, DPC micelles may provide a closer mimic to the lipid environment of cell fusion event. NMR spectra of VT18 were evaluated at different experimental conditions of varying peptide concentrations, detergent/peptide ratios, and temperatures. Sequence specific resonance assignment of VT18 was achieved by the use of 2-D  $^1\text{H}$ – $^1\text{H}$  TOCSY and  $^1\text{H}$ – $^1\text{H}$  NOESY experiments. Figure 3A shows the fingerprint region, delineating correlation between the backbone NH and C $^{\alpha}$ H resonances of each amino acid, of the 2-D TOCSY spectrum of VT18 in DPC micelles. As can be seen, the NH/C $^{\alpha}$ H cross-peaks are well resolved and identified for the 16 residues Y85-T101, except for the first residue V84 and residue P86, of VT18. The chemical shifts of proton resonances for the aliphatic side chains of amino acids were obtained either from TOCSY or NOESY spectra correlating NH resonances.

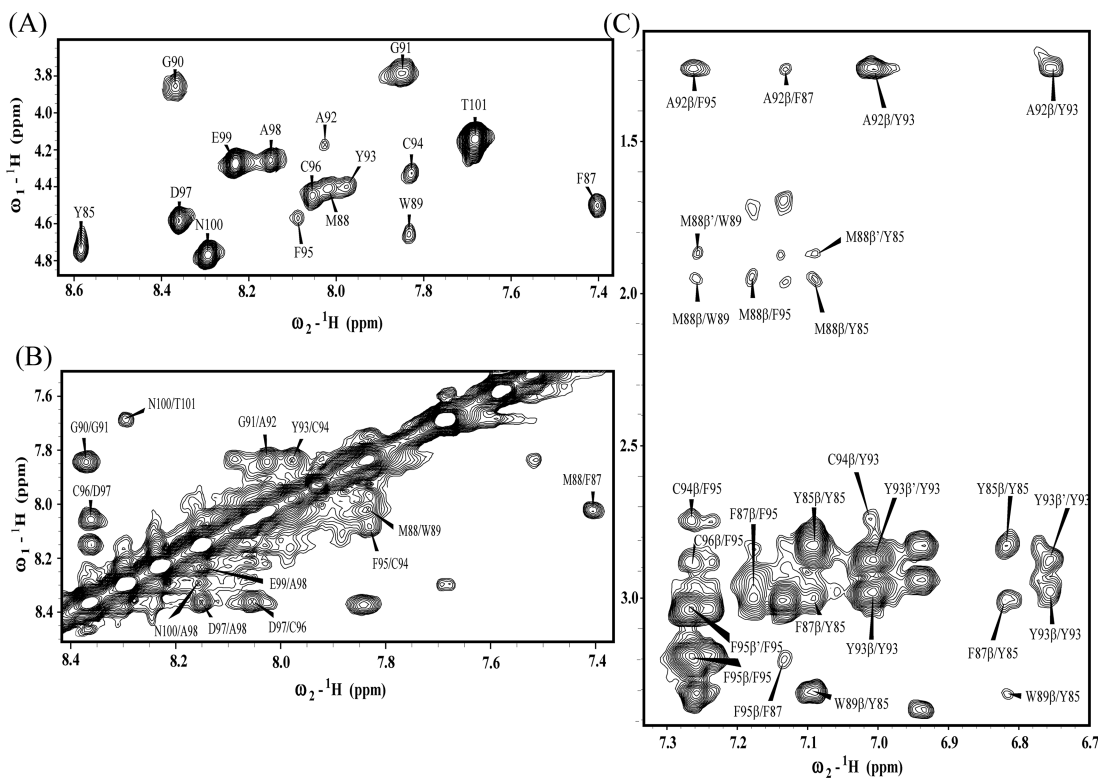


**Figure 3.** (A) The fingerprint region of the <sup>1</sup>H–<sup>1</sup>H 2-D TOCSY spectrum of VT18 showing correlation between the backbone NH and C<sup>α</sup>H resonances of amino acid residues. Selected regions of 2-D NOESY spectra of VT18 showing NOE connectivity between (B) backbone NH/NH resonances and (C) among the aromatic ring proton resonances with the aliphatic proton resonances. NMR spectra were acquired in aqueous solution, pH 5.0, containing 125 mM perdeuterated DPC at 310 K. Peptide concentration was kept at 0.5 mM.

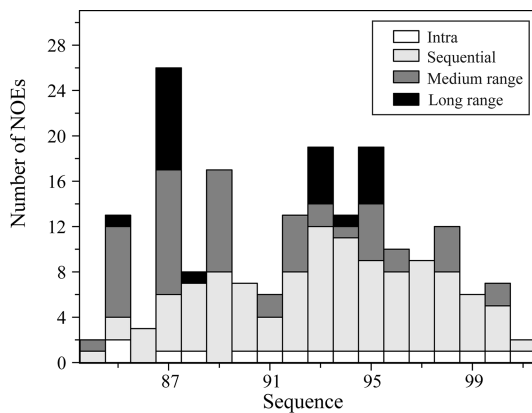


**Figure 4.** A bar diagram summarizing type (intra, sequential, medium-range, and long-range) and number of NOE contacts observed for each amino acid of VT18 in DPC micelles. The residue F87 delineated 26 NOEs including a number of long-range NOEs. Long-range NOE interactions were also detected for residues Y85, M88, Y93, C94, and F95.

The primary structure of VT18 contains as many as five aromatic residues, Y85, F87, W89, Y93, and F95. The ring proton resonances of these aromatic residues were identified from the intraresidue NOE contacts involving C<sup>α</sup>H and/or NH resonances. Analyses of 2-D <sup>1</sup>H–<sup>1</sup>H NOESY spectra of VT18 in detergent micelles revealed intense sequential C<sup>α</sup>H/NH NOEs and relatively less intense sequential NH/NH NOE for most of the residues (Figure 3B). In addition, the ring proton resonances of residues Y85, F87, W89, Y93, and Y95 were found to be involved in medium-range and long-range NOE

**Table 1. Summary of Structural Statistics of the 20 Lowest Energy Structures of VT18 Bound to DPC Micelles**

Distance restraints	
intraresidue ( $ i - j  = 0$ )	15
sequential ( $ i - j  = 1$ )	52
medium range ( $2 \leq  i - j  \leq 5$ )	26
long-range ( $( i - j  \geq 6)$ )	11
total NOE constraints	104
Dihedral angle constraints ( $\phi$ )	
	14
Distance restraints violations	
number of violations	16
average violation	$\leq 0.10 \text{ \AA}$
maximum violation	$\leq 0.30 \text{ \AA}$
Deviation from mean structure	
backbone atoms (N, C <sup>α</sup> , C') ( $\text{\AA}$ )	$0.24 \pm 0.12$
heavy atoms ( $\text{\AA}$ )	$0.55 \pm 0.12$
Ramachandran plot analysis <sup>a</sup>	
residues in the most favorable region	M88, A92, F95, C96, A98, E99
residues in the additionally allowed region	Y85, P86, W89, Y93, C94, D97, N100
residues in the generously allowed region	F87
residues in the disallowed region	None

<sup>a</sup>Data obtained from Procheck<sup>50</sup> of the nonglycyl residues. Two residues, V84 and T101, at the termini were excluded from analysis.

contacts (Figure 3C). In particular, long-range NOEs were detected between residues F87/F95, M88/F95, Y85/F95, F87/C94. Figure 4 shows a bar diagram summarizing type of NOEs of each residue of VT18 in DPC micelles. Notably, most of the

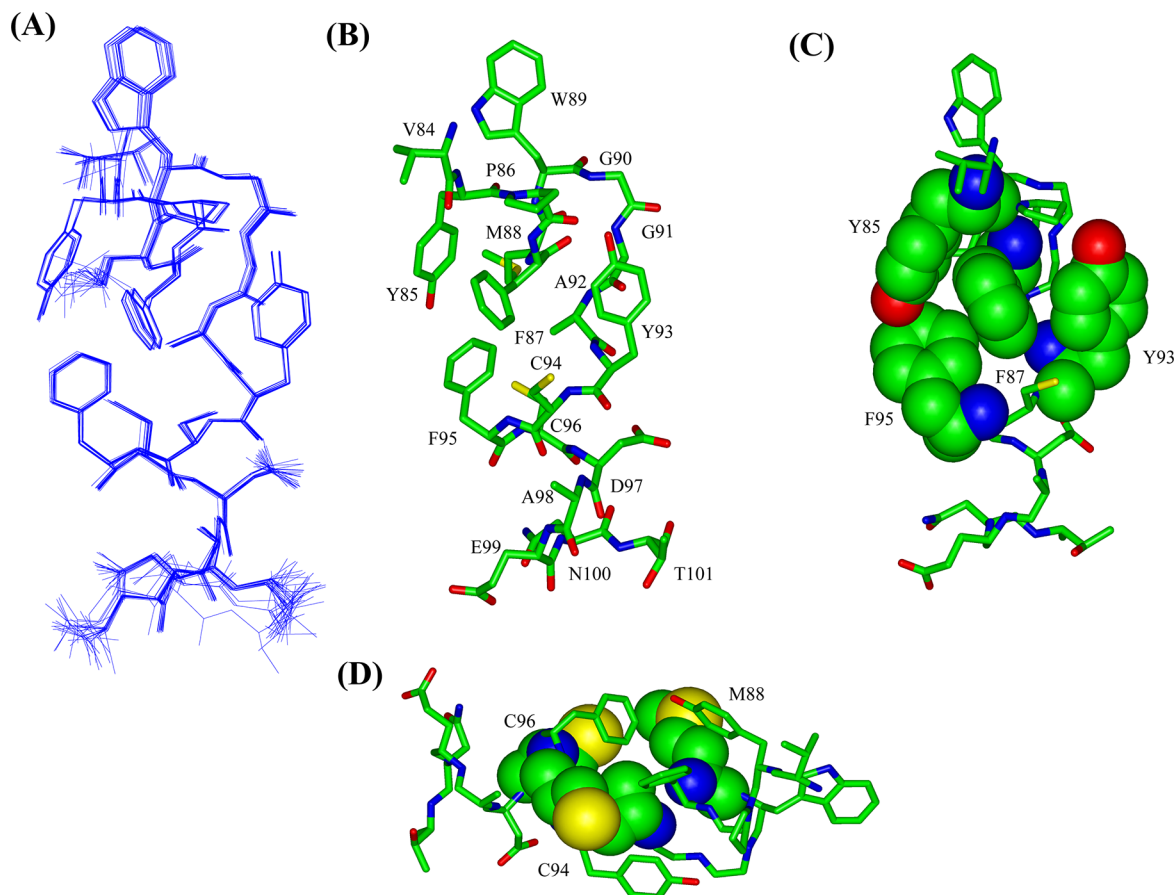


**Figure 5.** (A) Superposition of the backbone atoms ( $C^{\alpha}$ , N, and  $C'$ ) of 20 lowest energy structures of VT18 while bound to DPC micelles. (B) A representative structure of the DPC micelle-bound VT18 showing side chain disposition and topology. (C) A space-filling representation of the packing interactions among aromatic residues Y85, F87, Y93, and F95 in 3-D structure of VT18 in DPC micelles. In the aromatic cluster, residue F87 located centrally and critically involved in consolidating side chains of other aromatic residues by  $\pi/\pi$  stacking. (D) Orientation of the side chain of residues M88, C94, and C96 around the aromatic cluster of VT18 structure. Residues M88, C94, and C96 are shown in a space-filling model, and other residues are presented as stick. Figures were generated using INSIGHT II.

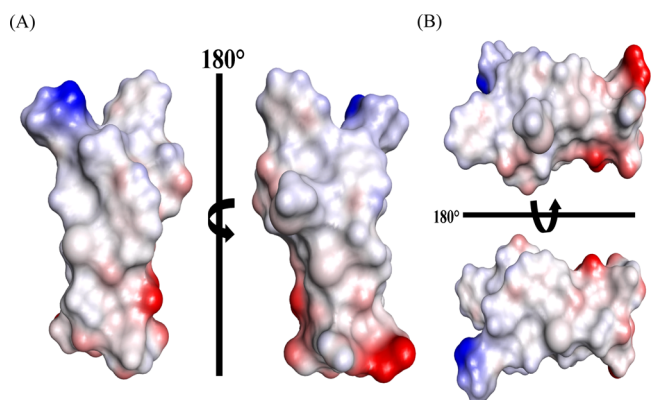


**Figure 6.** Electrostatic surface potential of VT18 fusion peptide bound to perdeuterated DPC-micelles showing for a representative structure (A) the front view and after a rotation of  $180^\circ$  along the  $z$ -axis and (B) the side view and after a rotation of  $180^\circ$  along the  $x$ -axis. Surfaces in red, blue and white stand for, respectively, negatively charged, positively charged and neutral residues. The figure was generated by PYMOL.

aromatic residues were involved in medium range and long-range NOE interactions, whereby F87 delineated as many as 26 NOEs including several long-range ones (Figure 4). By

contrast, residue W89 was characterized only by the medium range and sequential NOE interactions (Figure 4).

#### Three-Dimensional Structure of VT18 in DPC Micelles.

An ensemble of micelle-bound structure of the fusion peptide VT18 was determined utilizing 104 distance constraints including 26 medium-range and 11 long-range (Table 1). In order to limit conformational search, backbone dihedral angle  $\phi$  was restricted between  $-30^\circ$  to  $-120^\circ$  for the nonglycine residues. Figure 5A shows superposition of backbone atoms ( $C^{\alpha}$ , N, and  $C'$ ) of 20 lowest energy structures of the VT18 fusion peptide. The rmsd values for the backbone atoms and heavy atoms from the mean structure are found to be 0.24 Å and 0.55 Å, respectively (Table 1). The NMR structure of VT18 reveals an overall antiparallel orientation of the backbone topology around a type-I  $\beta$ -turn for the residues M88-W89-G90-G91 (Figure 5A,B). The nucleation of the  $\beta$ -turn is well supported by the diagnostic medium-range and intense sequential NOE contacts among the turn residues (Figures 3B and 4). The residue G90 occupying the i+2 position in the turn adopts  $\phi$ ,  $\psi$  values of  $-97^\circ$  and  $-3.9^\circ$ , respectively indicating the reversal of the polypeptide chain (Figure 5B). The backbone geometry of other residues, Y85-F87 and Y93-N100, of VT18 appears to be in extended conformations (Figure 5B). Strikingly, the 3-D structure of VT18 is well-defined in terms of mutual packing interactions among the side

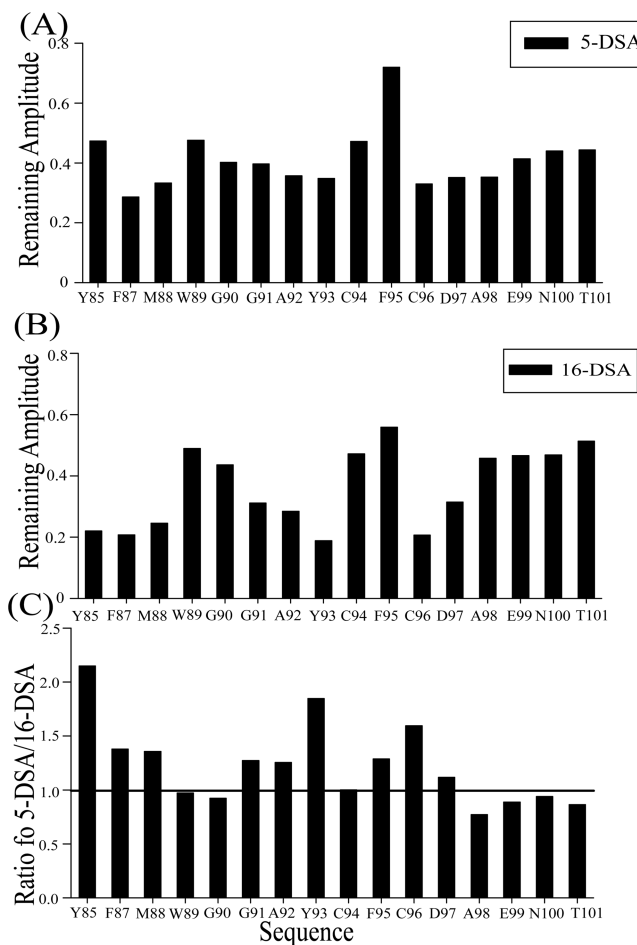


**Figure 7.** Bar diagrams showing the remaining signal amplitude observed for  $\text{NH}/\text{C}^{\alpha}\text{H}$  correlations in 2-D TOCSY spectra, after addition of paramagnetic lipid 5-DSA (A) and 16-DSA (B) in separate experiments, as a function of residues of VT18 fusion peptide. (C) Bar diagram shows the ratio of remaining signal amplitude, observed for  $\text{NH}/\text{C}^{\alpha}\text{H}$  correlations in 2-D TOCSY spectra, after addition of paramagnetic lipid 5-DSA and 16-DSA, as a function of residues of VT18 fusion peptide. A ratio of  $>1$  indicates a larger diminution of signal intensity by 16-DSA in comparison to that of 5-DSA, whereas a ratio of  $<1$  implies the opposite trend. Peptide samples were prepared in solution containing 125 mM perdeuterated DPC and TOCSY spectra were acquired either in the absence or in the presence of 1 mM doxyl lipids.

chains of aromatic residues, Y85, F87, Y93, and F95 at the N- and C-termini (Figure 5C). In the aromatic cluster, the side chain of residue F87 is centrally located and is involved in an extensive aromatic ring stacking interactions with Y85, Y93, and F95 (Figure 5C). The NH group of F87 remains in a close proximity with the aromatic side chains of residues Y93, F95 that may indicate potential amide- $\pi$  interactions. As a consequence, the chemical shift of the amide proton, 7.4 ppm, of F87 is shifted toward upfield in comparison to the other amide resonances (Figure 3A). The aromatic cluster is further complemented by the close packing interactions of the side chains of residues M88, A92, and C94 (Figure 5D). Notably, the side chain  $\text{S}-\text{CH}_3$  group of M88 intercalates between the aromatic rings of residues Y85 and F95 (Figure 5D). In addition, the side chain  $\text{CH}_2-\text{SH}$  group of C94 is also located at the edge of the phenyl ring of residue F87 (Figure 5D). The close proximity of  $\text{S}-\text{CH}_3$  and  $\text{CH}_2-\text{SH}$  groups of

M88 and C94, respectively, to the aromatic residues may represent aromatic-sulfur interactions in VT18 structure. Interestingly, intimate interside chain contacts between Met and/or Cys residues with aromatic residues could be seen in the 3-D structures of fusion peptides of HIV, SARS, dengue, and influenza viruses.<sup>27,29–31</sup> The electrostatic surface potential of the VT18 structure discloses a large hydrophobic region with only a limited negatively charged surface at the C-terminus of the molecule (Figure 6).

**Localization of VT18 in DPC Micelles.** Paramagnetic lipids, 5-doxy stearic acid (5-DSA), and 16-doxy stearic acid (16-DSA) were used to find out micelle insertion of the VT18 peptide. These paramagnetic or spin labeled doxyl lipids enhance relaxation of NMR active nuclei while incorporated into the lipid micelles.<sup>56,57</sup> In particular, micelles containing 5-DSA will induce broadening of NMR signals of amino acids located at the surface or within 3–4 carbon atoms from the site of spin label. On the other hand, residues deeply inserted or at the center of the micelle will experience signal attenuation in the presence of 16-DSA probe.<sup>56,57</sup> Two-dimensional  $^1\text{H}-^1\text{H}$  TOCSY spectra of VT18 were obtained in DPC micelles either in the absence or presence of 1 mM spin labeled doxyl lipids. Figure 7 shows remaining amplitude of the  $\text{NH}/\text{C}^{\alpha}\text{H}$  correlations of residues of VT18 in the presence of 5-DSA (panel A) and 16-DSA (panel B). Clearly, 5-DSA and 16-DSA both have attenuated intensity of the  $\text{NH}/\text{C}^{\alpha}\text{H}$  cross-peaks of residues of VT18, as a result of line broadening, however to a different extent. In order to compare the effect of the two PRE probes, the ratio of remaining amplitude of cross-peak intensity in 5-DSA and 16-DSA for each residues of VT18 is plotted in Figure 7C. As can be seen, a number of residues including Y85, F87, M88, G91, A92, Y93, F95, C96 of VT18 demonstrate a larger perturbation by 16-DSA, as  $5\text{-DSA}/16\text{-DSA} > 1$  (Figure 7C). In other words, these residues penetrate deeply toward the hydrophobic core of the DPC micelles. On the other hand,  $\text{NH}/\text{C}^{\alpha}\text{H}$  cross-peaks of residues W89, G90, A98, E99, N100, and T101 of the fusion peptide experienced a larger broadening by 5-DSA, as  $5\text{-DSA}/16\text{-DSA} < 1$  (Figure 7C). Thus, these residues of VT18 are located closer to the lipid headgroup or at the surface of the micelles. Collectively, these data indicated that the aromatic-hydrophobic core region of the VT18 structure is inserted into the DPC micelles. By contrast, residues W89 and G90 at the center of the  $\beta$ -turn and the polar and negatively charged C-terminal residues of VT18 are most likely orientated along the micellar surface.

#### Structural Comparison of the Type II Fusion Peptides.

Recently, 3-D structure of CHIKV fusion protein E1 has been determined, by X-ray crystallography, in complex with the receptor binding proteins E3 and E2.<sup>46</sup> In the crystal structure, the fusion peptide region (V84-T101) is buried at the interface of E1-E2 complex whereby side chains of His residues of E2 protein are potentially involved in hydrogen bonding with the main chain of the fusion peptide.<sup>46</sup> It may be instructive to compare the NMR derived DPC bound structure or the fusogenic structure of VT18 (Figure 8B) with that of the conformation deduced in the context of protein complexes (prefusion state) (Figure 8A). Figure 8C shows the superposition of the NMR derived structure and the crystal structure of the fusion peptide. Interestingly, in both the structures, deduced either in DPC micelles or in the context of E2 protein complexes, the type I  $\beta$ -turn for residues M88-W89-G90-G91 of the fusion peptide is well maintained along with the N- and C-termini pointing in an antiparallel orientation (Figure 8A–

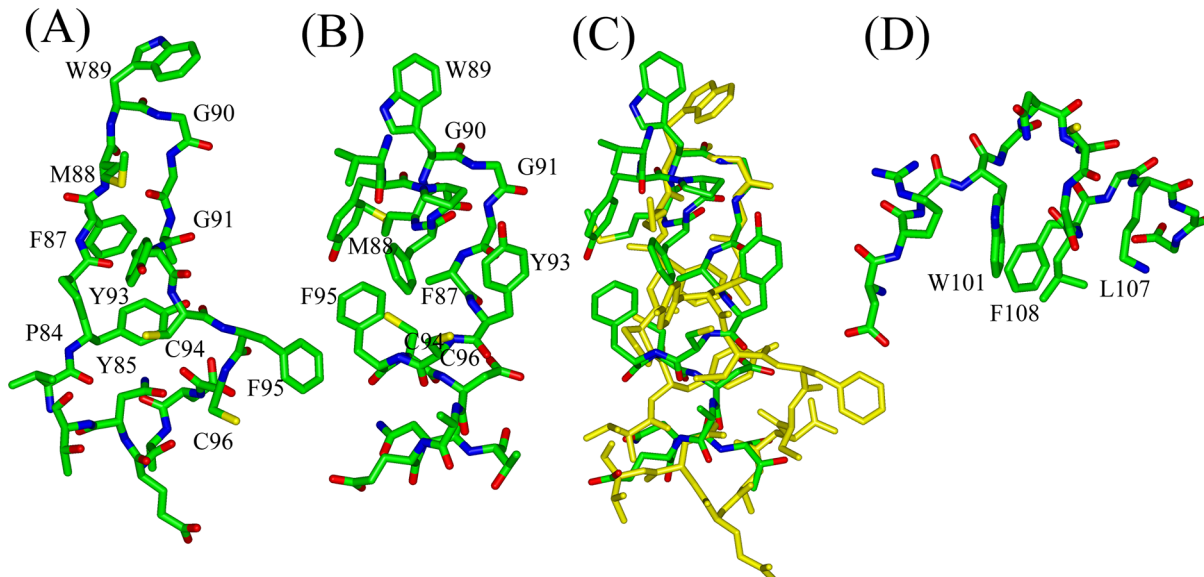


**Figure 8.** Comparison of conformations of the fusion peptides of CHIKV (A–C) and dengue virus (C) in different fusogenic states. (A) 3-D structure corresponding to the fusion peptide segment (V84-T101), determined by X-ray crystallography, in the full-length E1 protein in the prefusogenic state.<sup>45</sup> (B) The DPC-bound structure of the fusion peptide VT18 of CHIKV in fusogenic state solved by NMR spectroscopy in the current study. (C) Superposition of the NMR derived conformation with the X-ray structure of the fusion peptide of CHIKV. The X-ray structure of the fusion peptide is presented as a yellow stick. (D) The DPC-bound structure of the 15-residue fusion peptide of dengue virus solved by NMR spectroscopy.<sup>36</sup>

C). It may be worthwhile to consider that such a structural preservation of the  $\beta$ -turn conformation perhaps have important implications in membrane insertion and fusion. It is tempting to speculate that the  $\beta$ -turn residues of the fusion protein, upon pH-induced activation, make a facile insertion into the lipid membranes without loss of conformational entropy. On the other hand, the micelle-bound structure of the fusion peptide, VT18, markedly differs in terms of packing interactions of the aromatic side chains of residues Y85, F87, Y93, and F85 (Figure 8C). In the X-ray structure, there are diminished packing interactions among these aromatic side chains, in particular the side chain of residue F95 resided far apart from other aromatic residues (Figure 8C). In other words, in the lipidic environment of DPC micelles the fusion peptide has undergone a significant conformational reorganization for the aromatic residues (Figure 8B). In order to verify the plausible functional role of the aromatic residues and packing interactions, an analog peptide of VT18, whereby aromatic residues, F87, W89, and F95, were replaced with Ala, was examined for fusogenic activity. The mutated peptide did not exhibit any detectable lipid mixing activity, implying involvement of these aromatic residues in a structure–activity relationship (Supplementary Figure S2). However, role of the individual aromatic residue to the fusogenic activity and for the 3-D structure of VT18 peptide needs to be further investigated.

The NMR structure of 15-residue ( $D^{98}RGWGNGCGLFGKGG^{112}$ ) fusion peptide of dengue virus, the only structure known for a type II fusion peptide in lipid environments, was solved in DPC micelles.<sup>36</sup> The fusogenic conformation of dengue virus fusion peptide deduced in DPC micelles also demonstrated a close proximity of the side chains of aliphatic and aromatic residues. However, in the full-length E protein these side chains are not highly involved in packing interactions.<sup>36</sup> A replacement of aromatic residue W101 with Ala has caused a dramatic diminution of the fusogenic activity of the dengue virus fusion peptide.<sup>36</sup> It is

noteworthy that the overall 3-D structures, observed in DPC micelles, of the fusion peptides of CHIKV and dengue virus have remarkably differences (Figure 8B,D). Most notably, the 3-D structure of dengue virus fusion peptide is characterized by a limited hydrophobic surface consisting of residues W101, F108, and L107, correlating with a fewer number of nonpolar residues in the amino acid sequence. By contrast, the micelles-bound structure of VT18 fusion peptide displays a larger nonpolar surface with a fewer polar surface (Figure 6). This observation might implicate to a potentially different mode of insertion and membrane fusion of the fusion proteins of alphavirus and flavivirus.

## CONCLUSION

Viral fusion peptides are critical in promoting host-virus membrane fusion. A vast amount of work has been reported fusogenic activities and structures of fusion peptides derived from type I fusion proteins.<sup>14–16</sup> Collectively, these studies have provided important insight toward the membrane fusion process by type I fusion proteins. By contrast, fusion peptides of type II viral fusion proteins are inadequately explored for their structures and activities. The current study has demonstrated membrane fusion and interactions with zwitterionic liposomes of a type II fusion peptide, VT18, of CHIKV from alphavirus family. The atomic-resolution structure, determined in DPC micelles, of VT18 is defined by a hydrophobic core formed by the packing among aromatic and aliphatic residues. The hydrophobic core region of the fusion peptide is well inserted into the lipid micelles. These structural features of VT18 could be critical for the membrane fusion activity. We believe that the current work will provide a starting framework toward a better understanding, plausibly through mutational analyses of fusion protein, of the virus–host fusion by alphaviruses.

## ASSOCIATED CONTENT

### Supporting Information

Figures showing acrylamide quenching of VT18 peptide and fusogenic activity of the mutated VT18AAA peptide and a table of long-range NOE distance constraints. This material is available free of charge via the Internet at <http://pubs.acs.org>.

### Accession Codes

Atomic coordinates of the structures of VT18 have been deposited to the Protein Data Bank (PDB) with accession number 2RSW.

## AUTHOR INFORMATION

### Corresponding Author

\*E-mail: surajit@ntu.edu.sg. Fax: +65-6791-3856. Phone: +65-6316-7997.

### Present Address

<sup>#</sup>Bose Institute, Kolkata, India.

### Funding

This work is funded by a research grant (RG-49/10) from the Ministry of Education, Singapore.

### Notes

The authors declare no competing financial interest.

## ABBREVIATIONS USED

NMR, nuclear magnetic resonance; NOESY, nuclear Overhauser effect spectroscopy; TOCSY, total correlation spectroscopy; DPC, dodecylphosphocholine; NOE, nuclear Overhauser effect; DMPC, 1,2-dimyristoyl-sn-glycero-3-phosphocholine; CHIKV, Chikungunya virus

## REFERENCES

- (1) Skehel, J. J., and Wiley, D. C. (2000) Receptor binding and membrane fusion in virus entry: the influenza hemagglutinin. *Annu. Rev. Biochem.* 69, 531–569.
- (2) Eckert, D. M., and Kim, P. S. (2001) Mechanisms of viral membrane fusion and its inhibition. *Annu. Rev. Biochem.* 70, 777–810.
- (3) Harrison, S. C. (2005) Mechanism of membrane fusion by viral envelop proteins. *Adv. Virus. Res.* 64, 231–261.
- (4) Kielian, M., and Rey, F. A. (2006) Virus membrane-fusion proteins: more than one way to make a hairpin. *Nat. Rev. Microbiol.* 4, 67–76.
- (5) Weissenhorn, W., Hinza, A., and Gaudin, Y. (2007) Virus membrane fusion. *FEBS Lett.* 581, 2150–2155.
- (6) Earp, L. J., Delos, S. E., Park, H. E., and White, J. M. (2005) The many mechanisms of viral membrane fusion proteins. *Curr. Top. Microbiol. Immunol.* 285, 25–66.
- (7) Smith, A. E., and Helenius, A. (2004) How viruses enter animal cells. *Science* 304, 237–242.
- (8) Feng, Y., Broder, C. C., Kennedy, P. E., and Berger, E. A. (1996) HIV-1 entry cofactor: functional cDNA cloning of a seven-transmembrane, G protein-coupled receptor. *Science* 272, 872–877.
- (9) Lamb, R. A. (1993) Paramyxovirus fusion: a hypothesis for changes. *Virology* 197, 1–11.
- (10) Sieczkarski, S. B., and Whittaker, G. R. (2005) Viral entry. *Curr. Topics Microbiol. Immunol.* 285, 1–23.
- (11) Helenius, A., Kartenbeck, J., Simons, K., and Fries, E. (1980) On the entry of semliki forest virus into BHK-21 cells. *J. Cell Biol.* 84, 404–420.
- (12) Skehel, J. J., Bayley, P. M., Brown, E. B., Martin, S. R., Waterfield, M. D., White, J. M., Wilson, I. A., and Wiley, D. C. (1982) Changes in the conformation of influenza virus hemagglutinin at the pH optimum of virus-mediated membrane fusion. *Proc. Natl. Acad. Sci. U.S.A.* 79, 968–972.
- (13) Heinz, F. X., and Allison, S. L. (2000) Structures and mechanisms in flavivirus fusion. *Adv. Virus Res.* 55, 231–269.
- (14) Epand, R. M. (2003) Fusion peptide and the mechanisms of viral fusion. *Biochim. Biophys. Acta* 1614, 116–121.
- (15) Peisajovich, S. G., and Shai, Y. (2003) Viral fusion proteins: multiple regions contribute to membrane fusion. *Biochim. Biophys. Acta* 1614, 122–129.
- (16) Tamm, L. K. (2003) Hypothesis: spring-loaded boomerang mechanism of influenza hemagglutinin-mediated membrane fusion. *Biochim. Biophys. Acta* 1614, 14–23.
- (17) Vaney, M.-C., and Rey, F. A. (2011) Class II enveloped viruses. *Cell. Microbiol.* 13, 1451–1459.
- (18) Kielian, M. (2006) Class II virus membrane fusion proteins. *Virology* 344, 38–47.
- (19) Roche, S., Rey, F. A., Gaudin, Y., and Bressanelli, S. (2007) Structure of the prefusion form of the vesicular stomatitis virus glycoprotein G. *Science* 315, 843–848.
- (20) Peisajovich, S. G., Epand, R. F., Pritsker, M., Shai, Y., and Epand, R. M. (2000) The polar region consecutive to the HIV fusion peptide participates in membrane fusion. *Biochemistry* 39, 1826–1833.
- (21) Ghosh, J. K., Peisajovich, S. G., and Shai, Y. (2000) Sendai virus internal fusion peptide: structural and functional characterization and a plausible mode of viral entry inhibition. *Biochemistry* 39, 11581–11592.
- (22) Han, X., and Tamm, L. K. (2000) A host-guest system to study structure-function relationships of membrane fusion peptides. *Proc. Natl. Acad. Sci. U.S.A.* 97, 13097–13102.
- (23) Steinhauer, D. A., Wharton, S. A., Skehel, J. J., and Wiley, D. C. (1995) Studies of membrane fusion activities of fusion peptide mutants of influenza virus hemagglutinin. *J. Virol.* 69, 6643–6651.
- (24) Guillen, J., Perez-Berna, A. J., Moreno, M. R., and Villalain, J. (2008) A second SARS-CoV S2 glycoprotein internal membrane-active peptide. Biophysical characterization and membrane interaction. *Biochemistry* 47, 8214–8224.
- (25) Sainz, B., Jr., Rausch, J. M., Gallaher, W. R., Garry, R. F., and Wimley, W. C. (2005) The aromatic domain of the coronavirus class I viral fusion protein induces membrane permeabilization: putative role during viral entry. *Biochemistry* 44, 947–958.
- (26) Lai, A. L., and Tamm, L. K. (2007) Locking the kink in the influenza hemagglutinin fusion domain structure. *J. Biol. Chem.* 282, 23946–23956.
- (27) Han, X., Bushweller, J. H., Cafiso, D. S., and Tamm, L. K. (2001) Membrane structure and fusion-triggering conformational change of the fusion domain from influenza hemagglutinin. *Nat. Struct. Biol.* 8, 715–720.
- (28) Li, Y., and Tamm, L. K. (2007) Structure and plasticity of the human immunodeficiency virus gp41 fusion domain in lipid micelles and bilayers. *Biophys. J.* 93, 876–885.
- (29) Schibli, D. J., Montelaro, R. C., and Vogel, H. J. (2001) The membrane-proximal tryptophan-rich region of the HIV glycoprotein, gp41, forms a well-defined helix in dodecylphosphocholine micelles. *Biochemistry* 40, 9570–9580.
- (30) Lorieau, J. L., Louis, J. M., and Bax, A. (2010) The complete influenza hemagglutinin fusion domain adopts a tight helical hairpin arrangement at the lipid:water interface. *Proc. Natl. Acad. Sci. U.S.A.* 107, 11341–11346.
- (31) Jaroniec, C. P., Kaufman, J. D., Stahl, S. J., Viard, M., Blumenthal, R., Wingfield, P. T., and Bax, A. (2005) Structure and dynamics of micelle-associated human immunodeficiency virus gp41 fusion domain. *Biochemistry* 44, 16167–16180.
- (32) Chang, D. K., Cheng, S. F., Deo, V., and Yang, S. H. (2000) The amino-terminal region of the fusion peptide of influenza virus hemagglutinin HA2 inserts into sodium dodecyl sulfate micelle with residues 16–18 at the aqueous boundary at acidic pH. Oligomerization and the conformational flexibility. *J. Biol. Chem.* 275, 19150–19180.
- (33) Gregory, S. M., Harada, E., Liang, B., Delos, S. E., White, J. M., and Tamm, L. K. (2011) Structure and function of the complete internal fusion loop from ebolavirus glycoprotein 2. *Proc. Natl. Acad. Sci. U.S.A.* 108, 11211–11216.

- (34) Schmick, S. D., and Weliky, D. P. (2010) Major antiparallel and minor parallel  $\beta$  sheet populations detected in the membrane-associated human immunodeficiency virus fusion peptide. *Biochemistry* 49, 10623–10635.
- (35) Qiang, W., Sun, Y., and Weliky, D. P. (2009) A strong correlation between fusogenicity and membrane insertion depth of the HIV fusion peptide. *Proc. Natl. Acad. Sci. U. S. A.* 106, 15314–15319.
- (36) Melo, M. N., Sousa, F. J., Carneiro, F. A., Castanho, M. A., Valente, A. P., Almeida, F. C., Da-Poian, A. T., and Mohana-Borges, R. (2009) Interaction of the dengue virus fusion peptide with membranes assessed by NMR: the essential role of the envelope protein Trp101 for membrane fusion. *J. Mol. Biol.* 392, 736–746.
- (37) Her, Z., Kam, Y. W., Lin, R. T., and Ng, L. F. (2009) Chikungunya: a bending reality. *Microbes Infect.* 11, 1165–1176.
- (38) Schwartz, O., and Albert, M. L. (2010) Biology and pathogenesis of chikungunya virus. *Nat. Rev. Microbiol.* 8, 491–500.
- (39) Akahata, W., Yang, Z. Y., Andersen, H., Sun, S., Holdaway, H. A., Kong, W. P., Lewis, M. G., Higgs, S., Rossmann, M. G., Rao, S., and Nabel, G. J. (2010) A virus-like particle vaccine for epidemic Chikungunya virus protects nonhuman primates against infection. *Nat. Med.* 16, 334–338.
- (40) Strauss, J. H., and Strauss, E. G. (1994) The alphaviruses: gene expression, replication and evolution. *Microbiol. Rev.* 58, 491–562.
- (41) Wahlberg, J. M., Boere, W. A., and Garoff, H. (1989) The heterodimeric association between the membrane proteins of semliki forest virus changes its sensitivity to low pH during virus maturation. *J. Virol.* 63, 4991–4997.
- (42) Kielian, M., and Helenius, A. (1985) pH-induced alterations in the fusogenic spike protein of semliki forest virus. *J. Cell Biol.* 101, 2284–2291.
- (43) Wahlberg, J. M., Bron, R., Wilschut, J., and Garoff, H. (1992) Membrane fusion of Semliki Forest virus involves homotrimers of the fusion protein. *J. Virol.* 66, 7309–7318.
- (44) Lescar, J., Roussel, A., Wien, M. W., Navaza, J., Fuller, S. D., Wengler, G., Wengler, G., and Rey, F. A. (2001) The fusion glycoprotein shell of semliki forest virus: an icosahedral assembly primed for fusogenic activation at endosomal pH. *Cell* 105, 137–148.
- (45) Gibbons, D. L., Vaney, M. C., Roussel, A., Vigouroux, A., Reilly, B., Lepault, J., Kielian, M., and Rey, F. A. (2004) Conformational change and protein-protein interactions of the fusion protein of semliki forest virus. *Nature* 427, 320–325.
- (46) Voss, J. E., Vaney, M. C., Duquerroy, S., Vonrhein, C., Girard-Blanc, C., Crublet, E., Thompson, A., Bricogne, G., and Rey, F. A. (2010) Glycoprotein organization of chikungunya virus particles revealed by X-ray crystallography. *Nature* 468, 709–712.
- (47) Li, L., Jose, J., Xiang, Y., Kuhn, R. J., and Rossmann, M. G. (2010) Structural changes of envelope proteins during alphavirus fusion. *Nature* 468, 705–708.
- (48) Struck, D. K., Hoekstra, D., and Pagano, R. E. (1981) Use of resonance energy transfer to monitor membrane fusion. *Biochemistry* 20, 4093–4099.
- (49) Guntert, P., Mumenthaler, C., and Wuthrich, K. (1997) Torsion angle dynamics for NMR structure calculation with the new program DYANA. *J. Mol. Biol.* 273, 283–298.
- (50) Laskowski, R. A., Rullmann, J. A., MacArthur, M. W., Kaptein, R., and Thornton, J. M. (1996) AQUA and PROCHECK-NMR: programs for checking the quality of protein structures solved by NMR. *J. Biomol. NMR* 8, 477–486.
- (51) Wimley, W. C., and White, S. H. (1996) Experimentally determined hydrophobicity scale for proteins at membrane interfaces. *Nat. Struct. Biol.* 3, 842–848.
- (52) de Planque, M. R., Bonev, B. B., Demmers, J. A., Greathouse, D. V., Koeppe, R. E., Separovic, F., Watts, A., and Killian, J. A. (2003) Interfacial anchor properties of tryptophan residues in transmembrane peptides can dominate over hydrophobic matching effects in peptidelipid interactions. *Biochemistry* 42, 5341–5348.
- (53) Hiller, S., and Wagner, G. (2009) The role of solution NMR in the structure determinations of VDAC-1 and other membrane proteins. *Curr. Opin. Struct. Biol.* 19, 396–401.
- (54) Arora, A., and Tamm, L. K. (2001) Biophysical approaches to membrane protein structure determination. *Curr. Opin. Struct. Biol.* 11, 540–547.
- (55) Zamoon, J., Nitu, F., Karim, C., Thomas, D. D., and Veglia, G. (2005) Mapping the interaction surface of a membrane protein: unveiling the conformational switch of phospholamban in calcium pump regulation. *Proc. Natl. Acad. Sci. U. S. A.* 102, 4747–4752.
- (56) Van-den-Hooven, H., Spronk, C., Van-de-Kamp, M., Konings, R., Hilbers, C. W., and Van-de-ven, F. (1996) Surface location and orientation of lantibiotic nisin bound to membrane-mimicking micelles of dodecylphosphocholine and of sodium dodecylsulphate. *Eur. J. Biochem.* 235, 394–403.
- (57) Hilty, C., Wider, G., Fernandez, C., and Wüthrich, K. (2004) Membrane protein-lipid interactions in mixed micelles studied by NMR spectroscopy with the use of paramagnetic reagents. *ChemBioChem* 5, 467–473.